JOURNAL OF Materials CHEMISTRY

Synthesis, characterisation and performance of $(TiO_2)_{0.18}(SiO_2)_{0.82}$ xerogel catalysts

Mark A. Holland,*[a] David M. Pickup,[a] Gavin Mountjoy,[a] Edman S. C. Tsang,[c] Graham W. Wallidge,[a] Robert J. Newport[a] and Mark E. Smith[b]

[a]*School of Physical Sciences, University of Kent at Canterbury, UK CT2 7NR*
[b]*Department of Physics, University of Warwick, Coventry, UK CV4 7AL*
[c]*The Catalysis Research Centre, Department of Chemistry, University of Reading, UK RG6 6AD*

Received 30th June 2000, Accepted 1st August 2000
First published as an Advance Article on the web 26th September 2000

The synthesis of high surface area xerogels has been achieved using the sol–gel route. Heptane washing was used during the stages of drying to minimise capillary pressures and hence preserve pore structure and maximise the surface area. SAXS data have identified that heptane washing during drying, in general, results in a preservation of the pore structure and surface areas of up to 450 $m^2\ g^{-1}$. ^{17}O NMR showed that Ti is fully mixed into the silica network in all of the samples. XANES data confirm that reversible 4-fold Ti sites are more prevalent in samples with high surface areas, as expected. The calcined xerogels were tested for their catalytic activity using the epoxidation of cyclohexene with *tert*-butyl hydroperoxide (TBHP) as a test reaction, with excellent selectivities and reasonable percentage conversions. FT-IR spectroscopy has revealed that the catalytic activity is correlated with the intensity of the Si–O–Ti signal, after accounting for variations in Si–OH and Si–O–Si. The most effective catalyst was produced with heptane washing, a calcination temperature of 500 °C, and a heating rate of 5 °C min^{-1}.

Introduction

The sol–gel synthesis of glasses and ceramics offers a number of inherent advantages over traditional preparation techniques. The proper choice of the starting precursors allows production of high-purity, atomically mixed, homogeneous materials. Sol–gel derived mixed titania–silica oxide materials are of significant technological importance. They can be used as glasses with low thermal expansion coefficients.[1–4] Recently, sol–gel derived titania–silica oxides have been exploited for their potential use as catalysts and catalytic supports, and they are particularly suitable as epoxidation catalysts.[5,6]

The textural characteristics of sol–gel derived titania–silica oxides are strongly dependent on the processing of the gel. The sol–gel method offers the possibility of preparing solid materials with high surface areas, and controlled pore volumes and pore size distributions. Drying a newly prepared gel under ambient conditions often induces high capillary pressures, due to differential strain between the pore liquid and the gel network, which leads to a collapse of the porosity. Gels produced in this way are termed *xerogels*. Modified drying procedures can be used to produce textures more suitable for catalysis. Supercritical extraction, using an autoclave, avoids the capillary stress, and results in a mesoporous structure with large surface area. Gels produced in this way are termed *aerogels*. However, such an approach requires expensive autoclave equipment and can have detrimental effects on the gel structure so it is worthwhile to investigate alternative processing methods.

Previously, our group has extensively studied the structure of xerogels produced using routine drying.[7,8] In this work we use an alternative method, by initially ageing our xerogel samples for 10 days.[9] After this period, the samples were then washed in n-heptane for a further 10 days before drying was started. This solvent was chosen as it has a low surface tension, γ_{LV}, which according to eqn. (1) will reduce the capillary pressure, P_c, during drying and will hence preserve the pore structure.

$$P_c = \frac{-2\gamma_{LV}\cos\theta}{r} \quad (1)$$

Other terms defined in this equation are, θ, the contact angle and, r, the pore radius.[1]

The resulting xerogel samples were heat treated and studied using Small Angle X-Ray Scattering (SAXS), X-Ray Adsorption Near-Edge Structure spectroscopy (XANES), Extended X-Ray Absorption Fine Structure spectroscopy (EXAFS), Fourier Transform Infrared spectroscopy (FT-IR), Ultraviolet-Visible spectroscopy (UV-VIS) and ^{17}O Magic-Angle Spinning Nuclear Magnetic Resonance spectroscopy (^{17}O MAS NMR). The catalytic activity of the samples was assessed using the epoxidation of cyclohexene using *tert*-butyl hydroperoxide (TBHP). This enables a comprehensive investigation of the correlation between structural characteristics as a function of varying the synthesis conditions, and the resultant catalytic performance.

Experimental

Sample preparation

Samples were prepared with the following precursors: tetraethoxyorthosilicate (TEOS, Aldrich, 98%), titanium(IV) isopropoxide ($Ti(OPr^i)_4$, Aldrich, 97%), and isopropyl alcohol (IPA, Aldrich, 98%). The IPA acts as a mutual solvent, and HCl was used as a catalyst to promote the hydrolysis and condensation reactions. All reagents were loaded in a dry box and transferred using syringes to avoid absorption of moisture from the atmosphere.

During mixing of the precursors, the different rates of hydrolysis of the silicon and titanium alkoxides can cause phase separation, producing Ti-rich and Si-rich regions, which reduces the catalytic usefulness of the material.[10] We circumvent

DOI: 10.1039/b005408i

this problem using the method of Yoldas[11] which involves partially hydrolysing the Si alkoxide prior to mixing it with the Ti alkoxide. Before mixing with the Ti alkoxide, the TEOS was pre-hydrolysed for 2 hours using TEOS : IPA : H_2O in a 1 : 1 : 1 ratio, in the presence of an acid catalyst (pH of 1). The $Ti(OPr^i)_4$ and water were then added, such that the ratio, R, of water to alkoxide equals 2. With this ratio, complete hydrolysis can only occur by utilising water released from initial condensation. The mixtures were stirred while gelling and typical times to gelation were $\sim$100 hours. Samples for ^{17}O MAS NMR were prepared using enriched 10 mol% ^{17}O water (D-chem).

All gels were prepared with 18 mol% TiO_2. The resulting wet gels were separated into two equal quantities, and were initially left to age for 10 days. After this period, half of the yield was washed for two 5 day periods using 50 ml portions of n-heptane. The n-heptane was simply poured onto the xerogel surface and was allowed to exchange with the residual solvent in the pores of the sample. As mentioned previously, this process was undertaken twice to ensure complete solvent replacement with n-heptane in the pores. Following this, the residual n-heptane was decanted off and both samples were left to dry slowly (using a pinhole in the top of the otherwise sealed container to reduce the drying rate). The resultant xerogels were then finely ground, and heat treatments were performed at heating rates of 2 and 5 °C min^{-1}, with each set-point maintained for 2 h. Each sample was heated to intermediate temperatures up to a maximum of 750 °C. The following nomenclature will be used throughout to simplify sample identification: for example, a xerogel sample that has been heptane washed and heated to 500 °C at a rate of 2 °C min^{-1} will be labelled as "HW500(2)", whereas a non-washed xerogel after the same heat treatment would be labelled "NW500(2)", as shown in Table 1.

Surface area analysis

The specific surface area measurements were determined by nitrogen physisorption at 77 K using a Micromeritics ASAP 1000 instrument. The samples were out-gassed for 45 min at a temperature of 250 °C. BET surface areas were calculated in the relative pressure range between 0.05 and 0.2 assuming a cross-sectional area of 0.162 nm^2 for the nitrogen molecule.[12] Calibration of the equipment was undertaken by analysis of a silica with known surface area (500 $m^2 g^{-1}$).

SAXS

The SAXS experiments were carried out on Station 8.2 of the SRS, Daresbury Laboratory, UK. X-Rays of wavelength $\lambda = 1.54$ Å were used, with four sets of collimating slits to reduce slit scattering. Samples were contained in cells with kapton walls. Incident and transmitted X-ray intensities, I_0 and I_t, were measured using standard ion chambers before and after the sample (respectively). The SAXS intensity was recorded using a quadrant detector. A camera length of $L_c = 4.0$ m was used. The angular-scale for SAXS was calibrated from a reference sample of wet rat's tail collagen.

^{17}O MAS NMR

The ^{17}O MAS NMR spectra were acquired on a Chemagnetics CMX300 Infinity spectrometer. The spectra were collected at 40.7 MHz under MAS at typically 15.1 kHz, with a recycle delay of 1–2.5 s, using a Chemagnetics 4 mm double-bearing probe. The delay was sufficient to prevent saturation. A rotor-synchronised 90°–τ–180° echo sequence was applied with a short τ delay of 1 rotor period (66 μs) to overcome problems of probe ringing, thereby allowing the spectra to be phased correctly. The spectra were referenced externally to H_2O (0 ppm). Typically each spectrum was the result of 150 000–200 000 co-added scans and took *ca.* 36 h to collect.

XANES and EXAFS

Titanium K-edge X-ray absorption spectra were collected at Station 7.1 at the Daresbury Laboratory SRS using a Si [111] crystal monochromator and 50% harmonic rejection. Samples with a suitable optical thickness and high uniformity were prepared for the experiments by grinding and diluting in polyethylene or BN. Standard ionisation chambers, were placed in the beam path before and after the sample to measure incident and transmitted intensities I_0 and I_t respectively. EXAFS and XANES spectra were collected at the Ti K-edge (4966 eV[13]) in transmission mode at room temperature. A Ti metal foil placed in front of a third ion chamber was used for energy calibration.

UV-VIS spectrometry

UV-VIS spectra were acquired on a Unicam UV530 spectrometer, using a 76 mm integrating sphere in diffuse reflectance mode. The samples were scanned over the range 190–700 nm with a scan step of 0.5 nm, using an integrating time of 0.5 s. A blank calibrated Spectralon diffuse reflectance standard was used as a background.

FT-IR spectroscopy

Infrared spectra were recorded in diffuse reflectance mode using a Biorad FTS175C spectrometer controlled by Win-IR software. Samples were diluted (1 : 10 by weight) in dry KBr and scanned in the range 4000–400 cm^{-1} with a resolution of 4 cm^{-1}. Each spectrum was the result of summing 64 scans. The spectrum of dry KBr was taken for background subtraction.

Catalytic test reaction

0.2 g of the xerogel catalysts, prepared as above, and a magnetic stirrer were placed inside a 100 cm^3 three neck round bottom flask fitted with a thermometer, reflux condenser and a tapped dropping funnel. The apparatus was flushed with argon for 30 minutes before the addition of 10.0 cm^3 dichloromethane, 1.26 cm^3 pure cyclohexane (>99%, Sigma), and 1.0 cm^3 TBHP, (5.5 M in decane) *via* the dropping funnel where a 2 : 1 molar ratio of cyclohexene to TBHP is maintained at a

Table 1 Preparation parameters and catalytic performance for $(TiO_2)_{0.18}(SiO_2)_{0.82}$ xerogel samples[a]

Sample	Heat treatment/ °C	Rate of heat treatment/ °C min^{-1}	Washing	Surface area/ $m^2 g^{-1}$	Catalytic performance			
					Conversion (%)	$S_{epoxide}$ (%)	$S_{alcohol}$ (%)	S_{ketone} (%)
HW250(2)	250	2	Heptane	430	16.8	96.1	2.5	1.4
HW500(2)	500	2	Heptane	365	15.9	76.1	8.1	15.9
HW750(2)	750	2	Heptane	120	7.8	91.7	4.3	4.0
HW500(5)	500	5	Heptane	320	26.2	97.8	1.7	0.4
NW500(2)	500	2	None	182	8.7	>99	<0.5	<0.5
NW500(5)	500	5	None	25	19.5	91.6	3.9	4.5

[a]Errors: Surface area ± 10 $m^2 g^{-1}$, Catalytic performance ± 0.5%.

temperature of 45 °C. The mixture was then refluxed with continual stirring at about 45 °C for 24 h. The mixture was then allowed to cool, the supernatant was collected and centrifuged (4000 rpm, 4 min) and analysed.

Results and data analysis

SAXS

The raw data were divided by the detector response function and normalised to the incident beam flux and counting time. The adsorption correction was simplified by using the approximation $\theta \sim 0$, *i.e.* no path length variation. A background measurement of the empty container was subtracted. An approximate correction for variations in thickness between samples was made by multiplying $I_S(Q)$ by the factor $(\mu_s t_s)^{-1}$. These reduced data are shown in Fig. 1(a) for all six xerogel samples. The difference in shape between the heptane washed and non-washed xerogel samples is immediately apparent.

The angular dependence of scattering is described using the scattering vector, $Q = 4\pi\sin(\theta/2)/\lambda$, where θ is the scattering angle. The data analysis was used primarily to extract information about pore structures. For this reason the Guinier equation (eqn. (2)) was fitted to the data.

$$I(Q) = I_0 \exp\left(\frac{R_g{}^2 Q^2}{3}\right) \quad (2)$$

A power law background was used to take account of the behaviour at low Q due to scattering from the powder/void interface. Power law component of fits had exponents of −3 to −3.5. An estimate of the relative volume of the pores was calculated by expressing the ratio of I_0 to background. Fig. 1(b) shows the resultant fits for the Guinier equation and relevant power law for sample HW250(2). The results of the fitting for all samples are shown in Table 2.

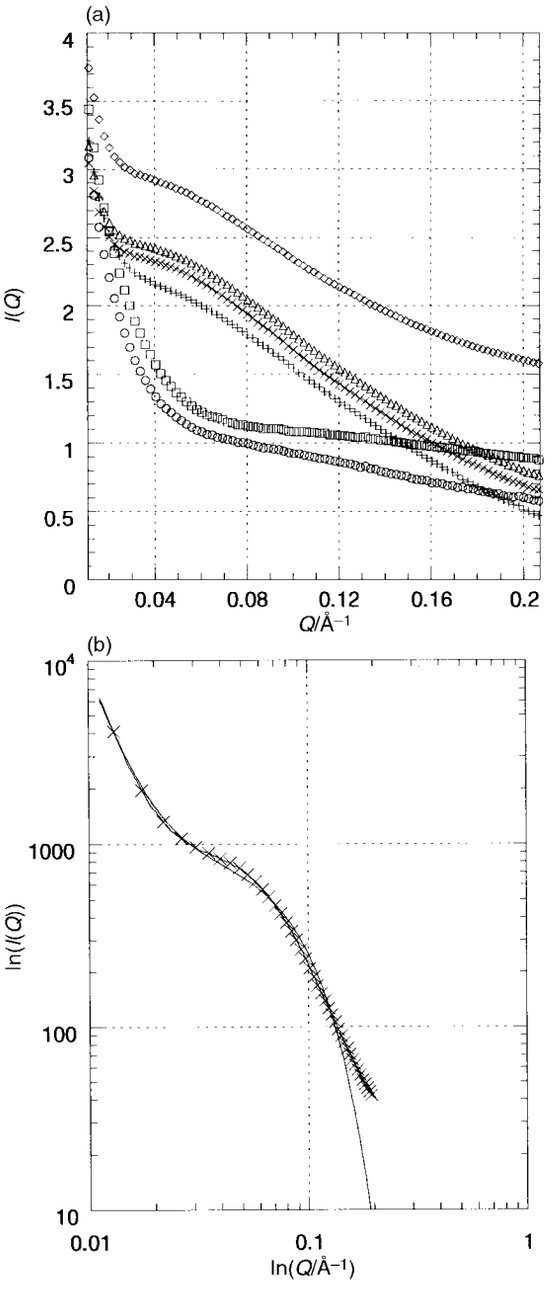

Fig. 1 a: SAXS plots for xerogel sample HW250(2) (◊), HW500(2) (×), HW750(2) (+), HW500(5) (△), NW500(2) (□), and NW500(5) (○). b: SAXS plot for sample HW250(2), including fitting of power law and Guinier equation. Experimental data, (solid line), and power law and Guinier fit, (×).

MAS NMR

The ^{17}O MAS NMR spectra of the enriched six xerogel samples are shown in Fig. 2. The spectra are dominated by a peak, with an isotropic chemical shift, ~0 ppm, and shows structure at negative shift due to a second order quadropole interaction.[14] This resonance has spinning sidebands from the MAS process at −325 and 350 ppm. By comparison with the ^{17}O signal from Si–O–Ti linkages at 190 ppm in the mineral fresnoite ($Ba_2TiSi_2O_8$)[15] and at 160 ppm in titanite ($CaTiSi_2O_5$),[16] the signals between 110–250 ppm have been attributed to co-ordination to oxygen. The resonance near 0 ppm is assigned to Si–O–Si linkages[17] with a contribution from Si–OH groups,[18] hence it is not a second order quadrupolar lineshape. Phase separated samples would exhibit two further resonances at 360 and 530 ppm due to OTi_4 and OTi_3 but no such resonances are apparent.[19]

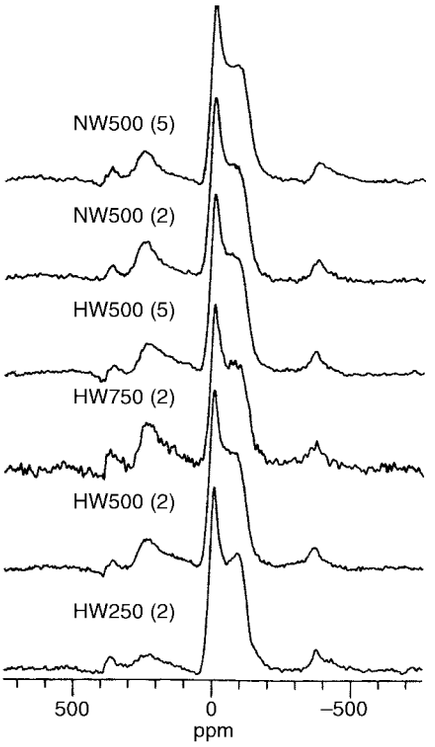

Fig. 2 ^{17}O MAS NMR spectra for xerogel samples.

Table 2 Experimentally derived structural parameters from SAXS, FT-IR, UV-VIS and EXAFS techniques[a]

	EXAFS parameters			XANES	UV-VIS	FT-IR	SAXS	
Sample	R_{TiO}	N_{TiO}	$2\sigma^2$/Å^2	Ti[4] irrev.	Abs. Edge/nm	I(Si–O–Ti)	Pore diameter/Å	Ratio of I_0 to backgd
HW250(2)	1.845	3.4	0.016	2	341	68	50	3.80
HW500(2)	1.850	2.7	0.012	14	360	77	54	1.40
HW750(2)	1.830	3.5	0.013	24	356	35	51	1.75
HW500(5)	1.845	2.5	0.009	15	340	97	54	1.05
NW500(2)	1.830	2.9	0.011	14	—	44	14	0.75
NW500(5)	1.845	2.9	0.014	21	—	91	21	0.30

[a]Errors: $R_{TiO} \pm 0.02$ Å, $N_{TiO} \pm 20\%$, $2\sigma^2 \pm 0.001$ Å^2, Ti[4] irrev. ± 5, Adsorption edge ± 3 nm, I(Si–O–Ti) ± 2, Pore diameter ± 2 Å, Ratio of I_0 to background ± 0.05.

EXAFS

The EXAFS data are analysed to obtain the absorbance, $\mu t = \ln(I_t/I_0)$, and then normalised absorbance $\chi(k) = (\mu t(k) - \mu t_{pre})/(\mu t_{post} - \mu t_{pre})$, where $\boldsymbol{k}$ is the photoelectron wave vector. The EXAFS data are fitted using the equation

$$\chi(k) = \mathrm{AFAC} \sum_j \frac{N_j}{kR_j^{\,2}} \left| f(\pi, k, R_j) \right| \mathrm{e}^{-2R_j/\lambda(k)} \mathrm{e}^{-2\sigma j^2 k^2} \sin(2kR_j + 2\delta(k) + \psi(k, R_j)) \quad (3)$$

AFAC is the proportion of electrons that undergo an EXAFS-type scatter and has been fixed at 0.9 for this analysis. N_j is the co-ordination number and R_j is the interatomic distance for the jth shell. The Debye–Waller factor is $A = 2\sigma^2$. $\delta(k)$ and $\psi(k, R_j)$ are the phase shifts experienced by the photoelectron, $f(\pi, k, R_j)$ is the amplitude of the photoelectron backscattering and $\lambda(k)$ is the electron mean free path.

The programs EXCALIB, EXBACK and EXCURV98 were used to extract the EXAFS signal and analyse the data. Least squares refinements of the structural parameters of our samples were carried out against the k^3 weighted $\chi(k)$ data in k-space using the single scattering approximation with $k_{min} = 3.0$ Å^{-1} and $k_{max} = 12.5$ Å^{-1} (*i.e.* up to 25 Å^{-1} using the conventional diffraction analysis definition of Q). The results of the refinements are reported in terms of the discrepancy index,

$$R = \frac{\int |\chi^T(k) - \chi^E(k)| k^3 \mathrm{d}k}{\int |\chi^E(k)| k^3 \mathrm{d}k} \quad (4)$$

Fig. 3 show the EXAFS fits and the corresponding Fourier transform for sample HW250(2).

The Ti K-edge EXAFS derived parameters for our xerogel samples are shown in Table 2. The fit errors and uncertainties are calculated within EXCURV98. The overall errors and uncertainties are likely to be greater due to other sources of inaccuracies, beyond fit statistics, such as the quality of background subtraction. Reasonable estimates of the total errors are ± 0.02 Å for nearest neighbour separations and $\pm 20\%$ for nearest neighbour coordinations.

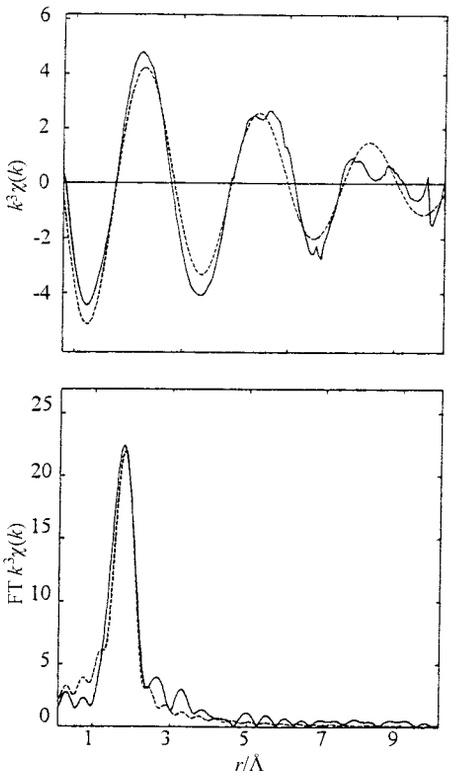

Fig. 3 Ti K-edge EXAFS for sample HW250(2): $k^3\chi(k)$ (top) and Fourier transform (bottom). Experimental data, solid line, and theoretical fit, dotted line.

XANES

The XANES spectra were processed according to our earlier work[20] to obtain $1 + \chi(E)$. Following the method of Farges *et al.*,[21] semi-quantitative information was extracted from the XANES spectra by least-squares fitting in the interval from 4900 to 4980 eV. We have previously applied this method to investigate Ti co-ordination in TiO_2–SiO_2 xerogels.[7] The fitting process involves using Lorentzian peak shapes to reflect the lifetime broadening of excited states. A single Lorentzian was used to model the dominant pre-edge peak, *i.e.* the peak of interest, and additional Lorentzians were used to model the remainder of the absorption edge. The results for the fitting of the Lorentzians for sample HW250(2) are shown in Fig. 4.

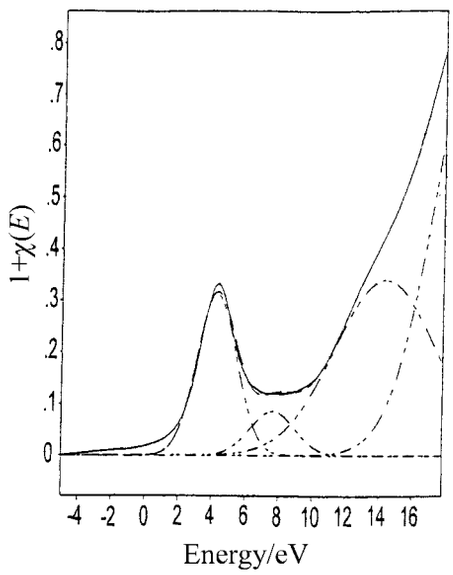

Fig. 4 XANES pre-edge and main edge features fitted using Lorentzian curves for hydrated sample HW250(2).

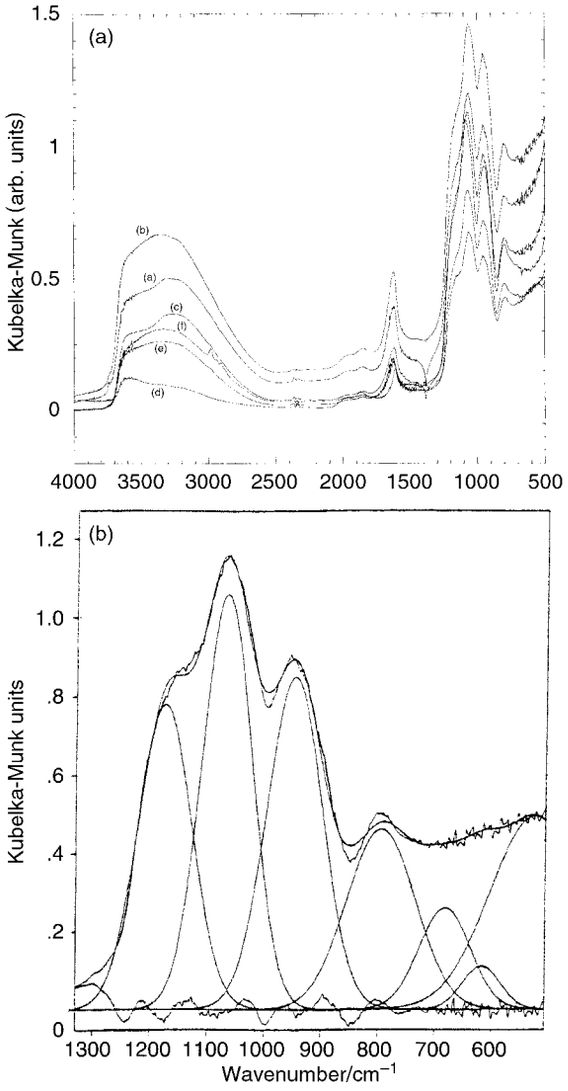

Fig. 5 (a) FT-IR spectra of xerogel samples: (a) HW250(2), (b) HW500(2), (c) HW750(2), (d) HW500(5), (e) NW500(2), (f) NW500(5). (b) FT-IR spectrum of sample HW250(2), expanded to show the silica/titania vibration region, including fitting of Gaussian curves.

Table 2 illustrates the relative amounts of stable 4-fold Ti in the xerogel network. As all of the Ti is known to be mixed into the silica network from NMR, the remaining Ti must be in the unstable 4-fold configuration. Unfortunately, owing to a problem with monochromator resolution on Station 7.1 which only became known after the experiment, the uncertainties are higher than normal.

FTIR spectroscopy

Fig. 5(a) shows the FT-IR spectra for all six xerogel samples. The peaks in the spectrum have been assigned by reference to the literature. Thus, the broad band in the region 3600–3000 cm^{-1} corresponds to the fundamental stretching vibrations of different hydroxyl groups.[22] The band at 3590 cm^{-1} is mainly due to stretching vibrations involving Si–OH groups and the band at 3350 cm^{-1} corresponds to adsorbed water. The band at 1610 cm^{-1} is assigned to the H–O–H bending vibration of water.

The region between 1450–650 cm^{-1} is characteristic of a silica network and is of particular interest to us, as evaluation of this region gives band positions and peak areas which provides a semi-quantitative estimate of the Si–O–Ti connectivity, or so-called Ti dispersion.[23,24] Fig. 5(b) represents, as an example, the IR spectrum for sample HW250(2) enlarged in this region. Within this region for all the samples the FTIR results suggest four bands which are here deconvolved into Gaussian curves, as illustrated in Fig. 5(b). The initial peak positions for the deconvolution were chosen at 800, 950, 1080 and 1220 cm^{-1}, respectively, and the peak positions then allowed to vary within a least squares iterative fitting routine. The positions and assignments of these vibrations are as follows: (i) the 800–810 cm^{-1} band is associated with the symmetric ν(Si–O–Si) stretching vibration;[25,26,1] (ii) the 940–960 cm^{-1} band arises from ν(Si–O–Ti) and ν(Si–[OH]) vibrations, (iii) the 1080–1105 cm^{-1} band arises from asymmetric ν(Si–O–Si) stretching vibrations (LO component),[25,26,1] and (iv) the 1180–1220 cm^{-1} band is associated with the TO component of the asymmetric ν(Si–O–Si) stretching vibrations.[1] The intensity of the Si–O–Ti connectivity (Ti dispersion), I(Si–O–Ti), is defined as

$$I(\text{Si–O–Ti}) \approx \frac{I(\text{Si–O–Ti, Si–[OH]})_{\sim 960\ \text{cm}^{-1}} - kI(\text{SiO–H})_{\sim 3590\ \text{cm}^{-1}}}{I(\text{Si–O–Si})_{\sim 1090\ \text{cm}^{-1}}} \quad (5)$$

The far right-hand side of this expression is a correction to the intensity at *ca.* 960 cm^{-1} to account for the contribution from an Si–OH resonance. We have estimated this contribution by measuring the ratio of the areas of the SiO–H ($\sim$3590 cm^{-1}) and Si–(OH) ($\sim$960 cm^{-1}) peaks in a pure SiO_2 xerogel. Thus k is defined as

$$k \approx \frac{I(\text{Si–[OH]})_{\sim 960\ \text{cm}^{-1}}}{I(\text{SiO–H})_{\sim 3590\ \text{cm}^{-1}}} \quad (6)$$

I(Si–O–Ti) represent a semiquantatitative measure of the relative number of Si–O–Ti linkages relative to the amount of Si–O–Si configurations. Note that the latter will be reduced in samples with large surface areas, and hence I(Si–O–Ti) will be enhanced in such samples. Table 2 displays these results alongside catalytic activity.

UV-VIS spectroscopy

The position of the UV adsorption edge was determined from the maximum inflection point in the UV spectra. The results for the four heptane washed samples are displayed in Table 1 (there were insufficient quantities of the non-washed samples remaining to obtain UV measurements).

Discussion

The general performance of the as-prepared catalysts shows reasonable percentage conversions, with sample HW500(5) peaking with a conversion of 26.2%. The selectivities of the samples are very good, with a minimum of 76.1% conversion to the epoxide. Five of the six samples show an epoxide selectivity in excess of 90%. By-products of unwanted alcohol and ketone components were extremely low, and in most cases were less than 5%, with the only exception being sample HW500(2) which displayed selectivities of 8.1 and 15.9% for the alcohol and ketone respectively. In the context of other work the supercritical drying technique (SCD) produces catalysts with selectivites in the region of 97–99% with conversions of $\sim$80%, which as expected exceeds the capability of our catalysts.[27] However, from an industrial perspective, the SCD technique is expensive as high temperature and pressure equipment is required.

The shape of the SAXS plot in the Q-region between $\sim$0.03 and 0.14 Å^{-1} can be regarded as a representation of the pore distribution for a given sample. The SAXS data reveal an immediate difference in pore structure between heptane washed and non-washed samples. For both of the non-washed samples, the SAXS plots in this region are concave, indicative of little or

no distinctive pore distribution. The results from the fitting of the Guinier equation reveal small pore sizes, with an average diameter of only $\sim$20 Å. This result is of course expected due to high capillary pressures present during routine drying and the consequent collapse of porosity. In the case of the heptane washed samples, as discussed earlier, the capillary pressures are reduced during drying resulting in a preservation of the external pore structure. The resultant SAXS plots, in the region $\sim$0.03–0.14 $Å^{-1}$ support this observation showing a smoothly humped curve, indicative of a distinct pore distribution. Fitting of the Guinier equation for the heptane washed samples yields much larger characteristic pore sizes, with an average diameter of $\sim$50 Å.

In addition, from the ratio of I_0 to the background which is representative of the relative abundance of pores, we conclude that there are more pores (by an order of magnitude) for the heptane washed samples compared to the non-washed samples. It should also be noted that the HW250(2), sample which displays the largest surface area (430 $m^2 g^{-1}$), also has the largest number of pores. In contrast, sample NW500(5) displaying the lowest surface area (25 $m^2 g^{-1}$) gives the lowest value for the abundance of pores.

The NMR data show no resonance at $\sim$530 ppm, this indicates no phase separation in any of the xerogel samples. Thus all samples have more-or-less complete mixing of Ti in the silica network. This is consistent with previous work which showed 18% samples were homogeneous up to 750 °C.[7] Note that the HW750(2) sample displays a very low catalytic activity, even though the intensity of Si–O–Ti linkages (estimated from the resonance at $\sim$220 ppm) is at least as strong as for the other samples. The reason for this is that the catalytic activity also depends upon whether the Si–O–Ti linkages are on an accessible surface. Interestingly, the SAXS data show that for the HW750(2) sample the pore structure collapses, due to the high calcination temperature; thus, although the number of Si–O–Ti linkages is high, there are few on a surface able to contribute to the catalytic activity.

The dominant central peak (near 0 ppm) consists of contributions from Si–OH and Si–O–Si; the quantification of the relative intensities of these two resonances is made difficult by the different quadrupolar coupling of ^{17}O in these two different environments, and deconvolution of these resonances cannot accurately be carried out without knowledge of the quadrupolar coupling constants. This problem can be overcome using Multiple Quantum NMR experiments,[28] which are beyond the scope of this paper. However, accurate quantification of Si–OH groups would be useful as it allows us to assess the hydrophilic/hydrophobic nature of a catalyst's surface.

The primary aim of the EXAFS experiments was to measure the Ti–O bond distances and co-ordination numbers. Unfortunately, the large uncertainties in EXAFS-determined nearest neighbour co-ordinations, $\pm$20%, limited the usefulness of this data. However, the average Ti–O distance from each sample is $\sim$1.83–1.85 Å, closer to 1.82 Å associated with 4-fold Ti than to 1.96 Å associated with 6-fold Ti sites.[7] This is consistent with NMR results which show complete mixing of Ti in the silica network.

As discussed above, Ti sites in the silica network differ in whether they are in the bulk, or on the surface. As shown in previous work, XANES has the ability to distinguish Ti sites with 4-fold co-ordination, and those with an additional two bonds to water groups which revert to purely 4-fold upon heating.[29] The latter, so-called reversible 4-fold sites, have been shown to be prevalent in xerogels with low heat treatment. Table 2 shows the XANES results for the catalyst samples, *i.e.* relative amount of irreversible 4-fold Ti. (Unfortunately, absolute values cannot reliably be generated because of the low resolution of the monochromator.) The remaining Ti is presumed to be in reversible 4-fold Ti sites, with co-ordination to water groups. Note that the XANES indicates irreversible 4-fold Ti is most prevalent in samples with low surface areas, and least prevalent in samples with high surface areas, as expected.

The FT-IR spectra were used to estimate *I*(Si–O–Ti), the so-called Ti dispersion, from the band that occurs at *ca.* 960 cm^{-1}. In fact, ^{17}O NMR has already shown that the mixing of Ti is very high in all samples. The quantity *I*(Si–O–Ti) derived from FTIR is in fact not a simple measure of Ti mixing. It also includes effects of surface area because it is normalised by dividing by *I*(Si–O–Si). The latter quantity will be reduced in samples with high surface area because they have less $Si(OSi)_4$ units, and the silica network is less rigid. A direct correlation is observed between *I*(Si–O–Ti) and the catalytic activity; a similar conclusion has been arrived at by other authors.[30]

The reason for the low surface area of sample NW500(5) and comparatively high activity is very interesting and is possibly attributed to the accessibility of the active Ti sites. Although this sample displays a high conversion percentage, it does show the second worst selectivity thus limiting its catalytic usefulness as unwanted products are formed during the epoxidation reaction. The activity of the catalyst is usually a function of the density of active sites on the surface, whereas the selectivity is influenced in a more complicated non-linear way by the number density. One such possibility is that the catalysis occurring on the surface of the NW500(5) sample is occurring by a different mechanism, due to a high density of active surface Ti sites. This would explain the high activity, even though the surface area of the sample is very low.

The achieved surface areas for the xerogels are quite high, up to $\sim$450 $m^2 g^{-1}$. Heptane washing, in general, preserves the pore structure of the xerogel and results in increased catalytic performance. Heat treatment using a higher rate. *i.e.* 5 rather than 2 °C min^{-1}, also appears to improve catalytic activity.

Conclusions

Good catalysts, with high selectivites and reasonable conversion percentages, have been synthesised using the sol–gel route with heptane washing techniques to maximise catalytic potential. Extensive structural characterisation has been carried out, and gives a clear picture of the effects of preparation conditions. ^{17}O NMR and EXAFS showed that all samples contain a homogeneous mixture of Ti in the silica network. SAXS data confirm that heptane washing leads to preservation of the pore structure and generally results in more effective catalysts with higher surface areas, since there are more accessible Si–O–Ti surface species. This is consistent with XANES results showing more irreversible 4-fold Ti sites in samples with low surface areas. The quantity *I*(Si–O–Ti) derived from FT-IR is in good correspondence with the catalytic activity.

Acknowledgements

The EPSRC is thanked for its support through grant GR/L28647. We also wish to thank E. R. H. van Eck for helpful discussions. Also thanked are Dr N. J. Terrill and Dr K. C. Cheung for help with X-ray experiments.

References

1 C. J. Brinker and G. W. Scherer, *Sol–Gel Science, The Physics and Chemistry of Sol–Gel Processing*, Academic Press, San Diego, 1990.
2 P. C. Schultz and H. T. Smyth, in *Amorphous Materials*, ed. E. W. Douglas and B. Ellis, Wiley, London, 1972.
3 M. E. Nordberg, *US Patent* 2 326 059, August 3, 1943.
4 T. Hayashi, H. Hattori and H. Saito, *J. Mater. Sci.*, 1983, **18**, 313.
5 M. Itoh, H. Hattori and K. J. Tanabe, *J. Catal.*, 1974, **35**, 225.
6 K. A. Jorgensensen, *J. Am. Chem. Soc.*, 1989, **3**, 89.
7 G. Mountjoy, D. M. Pickup, G. W. Wallidge, R. Anderson,

J. M. Cole, R. J. Newport and M. E. Smith, *Chem. Mater.*, 1999, **11**, 5.
8 R. Anderson, G. Mountjoy, M. E. Smith and R. J. Newport, *J. Non-Cryst. Solids*, 1998, **72–79**, 232.
9 S. Hæreid, E. Nilsen and M. Einarsrud, *J. Non-Cryst. Solids*, 1996, **204**, 228.
10 J. D. Basil and C. C. Lin, in *Ultrastructure Processing of Advanced Ceramics*, Wiley, New York, 1988.
11 B. E. Yoldas, *J.Non-Cryst. Solids*, 1980, **38**, 81.
12 D. C. M. Dutoit, M. Schneider and A. Baiker, *J. Catal.*, 1995, **153**, 165.
13 J. A. Bearden, *Rev. Mod. Phys.*, 1967, **39**, 125.
14 M. E. Smith, *Appl. Magn. Reson.*, 1993, **4**, 1.
15 P. J. Dirken, M. E. Smith and H. J. Whitfield, *J. Phys. Chem.*, 1995, **99**, 395.
16 P. S. Fiske and J. F. Stebbins, Department of Environmental Sciences, Stanford University, personal communication.
17 T. J. Bastow, A. F. Moodie, M. E. Smith and H. J. Whitfield, *J. Mater. Chem.*, 1993, **3**, 697.
18 T. M. Walter, G. L. Turner and E. Oldfield, *J. Magn. Reson.*, 1988, **76**, 106.
19 M. E. Smith and H. J. Whitfield, *J. Chem. Soc., Chem. Commun.*, 1994, 723.
20 D. M. Pickup, G. Mountjoy, G. W. Wallidge, R. Anderson, J. M. Cole, R. J. Newport and M. E. Smith, *J. Mater. Chem.*, 1999, **9**, 1299.
21 F. Farges, G. E. Brown and J. J. Rehr, *Geochim. Cosmochim. Acta*, 1996, **60**, 2023.
22 G. Orcel, J. Phalippou and L. L. Hench, *J. Non-Cryst. Solids*, 1986, **88**, 114.
23 R. Hutter, T. Mallat and A. Baiker, *J. Catal.*, 1995, **153**, 177.
24 A. Duran, A. Serna, V. Fornes and J. M. Fernandez-Navarro, *J. Non-Cryst. Solids*, 1986, **82**, 69.
25 M. Schraml-Marth, M. Walther, K. L. Wokaun, B. E. Handy and A. Baiker, *J. Non-Cryst. Solids*, 1991, **143**, 47.
26 M. E. Smith and E. R. H. van Eck, *Progr. NMR Spectrosc.*, 1999, **34**, 159.
27 R. Hutter, T. Mallat, A. Peterhams and A. Baiker, *J. Mol. Catal*, 1999, **138**, 241.
28 Z. Liu and R. J. Davis, *J. Phys. Chem.*, 1994, **98**, 1253.
29 J. Klaas, G. Schulz-Ekloff and N. I. Jaeger, *J. Phys. Chem. B*, 1997, **101**, 1205.
30 V. Luca, S. Djajanti and R. F. Howe, *J. Phys. Chem. B*, 1998, **102**, 10650.